

Spherical Authalic Energy Minimization for Area-Preserving Parameterization

Shu-Yung Liu [†] and Mei-Heng Yueh [†]

Abstract. We propose a new effective method called spherical authalic energy minimization (SAEM) for computing spherical area-preserving parameterizations of genus-zero surfaces. The proposed SAEM has solid theoretical support and guaranteed convergence. In addition, we develop a Riemannian bijective correction method to ensure the bijectivity of the produced mapping under mild assumptions. Numerical experiments showed that the SAEM effectively minimized area distortion with improved bijectivity compared to other state-of-the-art methods.

Keywords. simplicial surface, simplicial mapping, area-preserving parameterization, authalic energy, numerical optimization

AMS subject classifications. 65D18, 68U05, 68U01, 65D17

1 Introduction

Surface parameterization refers to the mapping of a surface in 3-dimensional space to a planar domain of a simple shape. This concept has been applied to surface resampling and registration [20, 26, 34, 38] in computer graphics, as well as brain flattening [5] and image processing for brain tumor segmentation [36, 37, 22, 23, 24]. Other classic applications and comprehensive overviews can be found in the survey papers [15, 32] and the lecture notes [18].

A desirable parameterization preserves the surface's geometric features as much as possible. However, achieving isometric (length-preserving) mapping is generally infeasible. Thus, most studies focus on angle-preserving (conformal) or area-preserving (authalic) mappings, while some attempt to balance both, approximating isometry.

For closed surfaces with no genus, the parameter domain is often the unit sphere. Several studies have explored spherical conformal parameterizations. Haker et al. [4, 16] used the finite element method to compute spherical conformal mappings by solving partial differential equations. However, their approach, which relies on stereographic projection, suffers from significant angular distortion near the north pole. To address this issue, Choi et al. [9] fixed the southern region and offset the angular distortion using a specific quasi-conformal mapping. Similarly, Choi et al. [7] and Yueh et al. [36, 21] improved the angular distortion in the northern region by harmonic mapping while keeping the southern region fixed. Alternatively, Nadeem et al. [30] applied Haker's method separately to the northern and southern hemispheres and welded the two regions with the least angular distortion.

While angle-preserving mappings maintain the local shape of a surface, they often result in significant area distortion. Area preservation is crucial for tasks such as brain morphometry. Several studies have focused on spherical area-preserving mappings for genus-zero surfaces. Moser [29] introduced a method by solving two differential equations in the sphere. Building on this, Dominitz et al. [11] computed optimal mass transportation (OMT) mappings by minimizing transportation costs. Subsequent studies extensively applied the OMT theory. Nadeem et al. [30] computed OMT mappings by minimizing a convex energy in Euclidean space via stereographic projection. Similarly, Choi et al. [6] computed OMT mappings in Euclidean space but first punctured a quadrilateral region at the bottom of the surface. In contrast, Cui et al. [10] developed a computational algorithm to compute OMT mappings directly on the sphere.

[†]Department of Mathematics, National Taiwan Normal University, Taipei, Taiwan (lii227857@gmail.com, yueh@ntnu.edu.tw)

In addition to the OMT approaches, Lyu et al. [27] employed density-equalizing methods combined with Riemannian projection to achieve area preservation. Yueh et al. [36, 19] introduced stretch energy minimization (SEM), solved using a combination of stereographic projection and the fixed-point method. The theoretical association between stretch energy and area preservation was established in [35]. This approach was further enhanced by incorporating a Riemannian gradient descent method with theoretical convergence [33].

Recently, Liu and Yueh [25] refined the energy minimization approach, significantly improving area preservation compared to the OMT method [40] and density-equalizing map [8] for simply connected open surfaces. However, this method has not been well-developed for genus-zero closed surfaces. In this paper, we adapt and modify this energy minimization approach for spherical area-preserving parameterization. We expect that it will demonstrate superior efficacy compared to state-of-the-art methods, as observed in the case of open surfaces.

The paper is organized as follows. In Section 2, we highlight the contributions of our work. Section 3 introduces the mathematical background. Section 4 presents the modified objective functional for improved numerical performance, with the associated iterative method detailed in Section 5. Section 6 discusses a post-processing technique to ensure bijectivity for challenging cases. Numerical results are presented in Section 7. Finally, we discuss our proposed method compared with existing approaches in Section 8 and conclude in Section 9.

2 Contributions

The contributions of this work are threefold:

- (i) We propose a novel objective functional, the spherical authalic energy, which improves bijectivity during optimization for spherical area-preserving parameterization of genus-zero closed surfaces.
- (ii) We develop an efficient energy minimization method with theoretically guaranteed convergence, demonstrating superior performance in both accuracy and efficiency compared to state-of-the-art methods in numerical experiments.
- (iii) We introduce a Riemannian bijective correction method with strong theoretical support, which is capable of resolving hundreds of folding triangles, effectively addressing challenging cases.

3 Mathematical background

In this section, we introduce some basic mathematical concepts closely related to our work.

3.1 Simplicial mapping

A smooth surface can be approximated by a simplicial surface, namely, a triangular mesh, denoted as $\mathcal{M} = (\mathcal{V}(\mathcal{M}), \mathcal{E}(\mathcal{M}), \mathcal{F}(\mathcal{M}))$, where

$$\mathcal{V}(\mathcal{M}) = \{v_\ell = (v_\ell^1, v_\ell^2, v_\ell^3) \in \mathbb{R}^3\}_{\ell=1}^n, \quad (3.1a)$$

$$\mathcal{F}(\mathcal{M}) = \{\tau_s = [v_{i_s}, v_{j_s}, v_{k_s}] \subset \mathbb{R}^3 \mid v_{i_s}, v_{j_s}, v_{k_s} \in \mathcal{V}(\mathcal{M})\}_{s=1}^m, \quad (3.1b)$$

and

$$\mathcal{E}(\mathcal{M}) = \{[v_i, v_j] \subset \mathbb{R}^3 \mid [v_i, v_j, v_k] \in \mathcal{F}(\mathcal{M})\}, \quad (3.1c)$$

are sets of n vertices, m oriented triangular faces and edges, respectively, in which the bracket $[v_{i_s}, v_{j_s}, v_{k_s}]$ denotes a 2-simplex, i.e., a triangle with vertices being $v_{i_s}, v_{j_s}, v_{k_s}$.

A spherical simplicial mapping $f : \mathcal{M} \rightarrow \mathbb{S}^2$ is a piecewise affine mapping from simplicial surface \mathcal{M} into spherical simplicial complex $f(\mathcal{M}) = (\mathcal{V}(f(\mathcal{M})), \mathcal{E}(f(\mathcal{M})), \mathcal{F}(f(\mathcal{M})))$, in which $\mathcal{V}(f(\mathcal{M}))$, $\mathcal{E}(f(\mathcal{M}))$, and $\mathcal{F}(f(\mathcal{M}))$ are vertices, edges, and triangular faces of $f(\mathcal{M})$ as in (3.1), respectively.

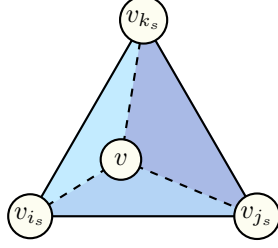


Fig. 1. An illustration of the barycentric coordinates on a triangular face.

The simplicial mapping can be determined by the mapping of its vertices. Any point on a triangular face of the spherical simplicial complex can be represented using barycentric coordinates. In other words, f is a piecewise affine mapping that satisfies

$$f(v_i) = (f_i^1, f_i^2, f_i^3)^\top, \quad \forall v_i \in \mathcal{V}(\mathcal{S}),$$

and

$$f|_{\tau_s}(v) = \frac{1}{|\tau_s|} \left(|[v, v_{j_s}, v_{k_s}]| f(v_{i_s}) + |[v_{i_s}, v, v_{k_s}]| f(v_{j_s}) + |[v_{i_s}, v_{j_s}, v]| f(v_{k_s}) \right),$$

for every $\tau_s \in \mathcal{F}(\mathcal{S})$, where the absolute value of the simplex denotes the area of that simplex (see Figure 1).

3.2 Authalic mapping

Given a simplicial surface \mathcal{M} . A simplicial map $f : \mathcal{M} \rightarrow \mathbb{S}^2$ is said to be authalic or area-preserving if

$$|f(\tau)| = c |\tau| \quad \text{for all } \tau \in \mathcal{F}(\mathcal{M})$$

for some constant $c \in \mathbb{R}$. The ratio of the area of a triangle in the domain to its area in the image under the mapping is called the stretch factor, denoted as

$$\sigma_{f^{-1}}(\tau) = \frac{|\tau|}{|f(\tau)|}.$$

It has been shown in [39, Theorem 1] that the stretch factor

$$\sigma_{f^{-1}}(\tau) = \sqrt{\det(\mathbf{I}_{f^{-1}}|_{f(\tau)})}, \quad (3.2)$$

where $\mathbf{I}_{f^{-1}}$ is the first fundamental form of f^{-1} . As a result, authalic maps satisfy the constant area element property, which is consistent with the concept in classical differential geometry.

3.3 Authalic energy functional

In the previous work, Yueh [39] defined the stretch energy E_S , measuring the area-preserving property for a given simplicial mapping $f : \mathcal{M} \rightarrow \mathbb{R}^2$, given by

$$E_S(f) = \sum_{\tau \in \mathcal{F}(\mathcal{M})} \frac{|f(\tau)|^2}{|\tau|}. \quad (3.3)$$

From the identity of the stretch factor (3.2), the stretch energy is equivalent to

$$E_S(f) = \sum_{\tau \in \mathcal{F}(\mathcal{M})} \det(\mathbf{I}_{f^{-1}}|_{f(\tau)})^{-1} |\tau| = \sum_{\tau \in \mathcal{F}(\mathcal{M})} \int_{\tau} \det(\mathbf{I}_{f^{-1}}|_{f(\tau)})^{-1} dA.$$

It has been shown that the lower bound of $E_S(f)$ is the image area $|f(\mathcal{M})|$. Under the assumption that the surface area is equal to the image area, the minimal value of $E_S(f)$ occurs when f is an area-preserving mapping [35, Theorem 3.3].

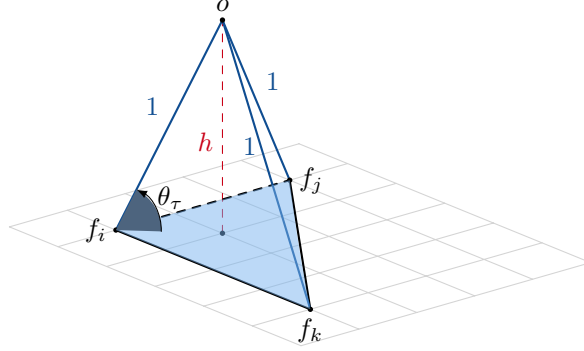


Fig. 2. The illustration of the tetrahedron by $[o, f_i, f_j, f_k]$ constructed by the triangle $[f_i, f_j, f_k]$ and the origin o .

By Cauchy–Schwartz inequality, Liu and Yueh [25] relax the image area constraint and propose the authalic energy

$$E_A(f) = \frac{|\mathcal{M}|}{|f(\mathcal{M})|} E_S(f) - |f(\mathcal{M})|. \quad (3.4)$$

The lower bound of $E_A(f)$ is zero and the minimal value occurs when f is area-preserving [25, Theorem 1]. This objective function allows the change of the image area so that the boundary points can be updated in numerical optimization procedures.

4 Objective energy functional

Authalic energy minimization is an efficient method for achieving area-preserving mappings, as demonstrated in unit disk parameterization for simply connected open surfaces [25]. However, it faces difficulties when applied to spherical parameterization for genus-zero closed surfaces. In this section, we introduce the challenge of the authalic energy and propose our modified objective functional, the spherical authalic energy.

4.1 Spherical authalic energy functional

Noting that E_A in (3.4) contains a negative image area term $f(\mathcal{M})$, minimizing E_A would also maximize $f(\mathcal{M})$ and result in folding triangles on the image. Due to this fact, the orientation of the triangle area should be taken into account. However, accounting for face orientation in the spherical image introduces discontinuity, because when triangles flip their normals from outward to inward on the sphere, their areas become negative without passing through zero. This would significantly affect the optimization process. To address this issue, we modify the energy functional as follows. Rather than considering the area of the spherical image face $f(\tau) = [f_i, f_j, f_k]$, we instead consider the associated tetrahedron formed by $[o, f_i, f_j, f_k]$, where o is the origin, as illustrated in Figure 2. As the spherical orientation of the triangle $[f_i, f_j, f_k]$ changes, the volume $[o, f_i, f_j, f_k]$ continuously varies from a positive value to a negative one. This modification provides the benefit that the orientations of triangles are taken into account and the functional remains continuous. Based on this concept, we define the spherical authalic energy functional as

$$E_{\mathbb{A}}(f) = \frac{|\mathcal{M}|}{3\mathcal{V}(f)} E_S(f) - 3\mathcal{V}(f), \quad (4.1)$$

where E_S is the stretch energy defined in (3.3) and \mathcal{V} is the volume measurement, defined as

$$\mathcal{V}(f) = \sum_{[v_i, v_j, v_k] \in \mathcal{F}(\mathcal{M})} |[o, f_i, f_j, f_k]|. \quad (4.2)$$

Noting that the area of the unit sphere is 4π , which is equal to 3 times the volume of the unit sphere, the spherical authalic energy functional $E_{\mathbb{A}}$ in (4.1) is an approximation to the authalic energy functional E_A in (3.4). The detailed statement is provided in the following theorem.

Theorem 1. *Given a simplicial surface \mathcal{M} . Let $f : \mathcal{M} \rightarrow \mathbb{S}^2$ be an orientation-preserving simplicial map and ε_f be the maximal edge length of $f(\mathcal{M})$. The spherical authalic energy (4.1) satisfies the estimate*

$$|E_{\mathbb{A}}(f) - E_A(f)| \leq \left(1 + \frac{E_S(f)|\mathcal{M}|}{3\mathcal{V}(f)|f(\mathcal{M})|}\right) |f(\mathcal{M})| \left(1 - \sqrt{1 - \varepsilon_f^2}\right), \quad (4.3)$$

where authalic energy $E_{\mathbb{A}}$ and stretch energy E_S are defined as (3.4) and (3.3), respectively. Moreover, if f is an area-preserving mapping, then

$$0 \leq E_{\mathbb{A}}(f) \leq \left(1 + \frac{|f(\mathcal{M})|}{3\mathcal{V}(f)}\right) |f(\mathcal{M})| \left(1 - \sqrt{1 - \varepsilon_f^2}\right). \quad (4.4)$$

Proof. From (3.4) and (4.1), we have

$$\begin{aligned} E_{\mathbb{A}} - E_A &= \left(\frac{|\mathcal{M}|}{3\mathcal{V}(f)} E_S(f) - 3\mathcal{V}(f)\right) - \left(\frac{|\mathcal{M}|}{|f(\mathcal{M})|} E_S(f) - |f(\mathcal{M})|\right) \\ &= E_S(f)|\mathcal{M}| \left(\frac{1}{3\mathcal{V}(f)} - \frac{1}{|f(\mathcal{M})|}\right) + (|f(\mathcal{M})| - 3\mathcal{V}(f)) \\ &= E_S(f)|\mathcal{M}| \left(\frac{|f(\mathcal{M})| - 3\mathcal{V}(f)}{3\mathcal{V}(f)|f(\mathcal{M})|}\right) + (|f(\mathcal{M})| - 3\mathcal{V}(f)) \\ &= \left(1 + \frac{E_S(f)|\mathcal{M}|}{3\mathcal{V}(f)|f(\mathcal{M})|}\right) (|f(\mathcal{M})| - 3\mathcal{V}(f)). \end{aligned} \quad (4.5)$$

For each $f(\tau) = [f_i, f_j, f_k]$, $[o, f_i, f_j, f_k]$ is the isosceles tetrahedron (see Figure 2) with the volume

$$|[o, f_i, f_j, f_k]| = \frac{h}{3}|f(\tau)|, \quad (4.6)$$

where h is the altitude with respect to the base $f(\tau)$. Let θ_τ be the angle between the edge $[o, f(v_i)]$ and the base $f(\tau)$ for some vertex $f(v_i)$. The altitude h can be regarded as the $\sin \theta_\tau$ and $\cos \theta_\tau$ is the line segment between $f(v_i)$ and orthocenter. Then, we have

$$h = \sin \theta_\tau = \sqrt{1 - \cos^2 \theta_\tau} \geq \sqrt{1 - \varepsilon_f^2}. \quad (4.7)$$

Therefore, by (4.6) and (4.7), we obtain

$$\begin{aligned} |f(\mathcal{M})| - 3\mathcal{V}(f) &= \sum_{\tau \in \mathcal{F}(\mathcal{M})} |f(\tau)| - \sum_{\tau \in \mathcal{F}(\mathcal{M})} |f(\tau)| h \\ &\leq \sum_{\tau \in \mathcal{F}(\mathcal{M})} |f(\tau)| - \sum_{\tau \in \mathcal{F}(\mathcal{M})} |f(\tau)| \sqrt{1 - \varepsilon_f^2} \\ &= |f(\mathcal{M})| \left(1 - \sqrt{1 - \varepsilon_f^2}\right). \end{aligned} \quad (4.8)$$

As a result, by (4.5) and (4.8), we obtain

$$\begin{aligned} E_{\mathbb{A}} - E_A &= \left(1 + \frac{E_S(f)|\mathcal{M}|}{3\mathcal{V}(f)|f(\mathcal{M})|}\right) (|f(\mathcal{M})| - 3\mathcal{V}(f)) \\ &\leq \left(1 + \frac{E_S(f)|\mathcal{M}|}{3\mathcal{V}(f)|f(\mathcal{M})|}\right) |f(\mathcal{M})| \left(1 - \sqrt{1 - \varepsilon_f^2}\right), \end{aligned}$$

which conclude (4.3).

Additionally, since $\sin \theta_\tau \leq 1$ for all $\tau \in \mathcal{F}(\mathcal{M})$, $3\mathcal{V}(f) \leq |f(\mathcal{M})|$ and thus $E_{\mathbb{A}}(f) \geq E_A(f)$. If f is area-preserving, $E_A(f) = 0$ and $E_S(f) = |f(\mathcal{M})|^2/|\mathcal{M}|$. Consequently, by (4.3), we can conclude (4.4) as

$$\begin{aligned} 0 \leq E_{\mathbb{A}}(f) &\leq \left(1 + \frac{E_S(f)|\mathcal{M}|}{3\mathcal{V}(f)|f(\mathcal{M})|}\right) |f(\mathcal{M})| \left(1 - \sqrt{1 - \varepsilon_f^2}\right) + E_A(f) \\ &\leq \left(1 + \frac{|f(\mathcal{M})|}{3\mathcal{V}(f)}\right) |f(\mathcal{M})| \left(1 - \sqrt{1 - \varepsilon_f^2}\right). \end{aligned}$$

□

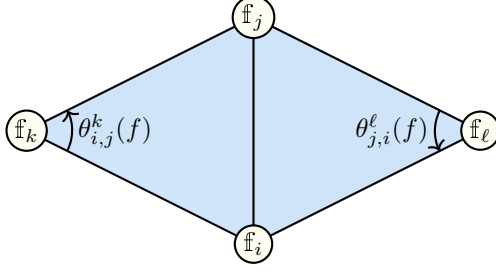


Fig. 3. An illustration of the cotangent weight defined on the surface $f(\mathcal{M})$.

It is important to emphasize that while $E_{\mathbb{A}}$ approximates E_A , the convergence behavior of minimizing $E_{\mathbb{A}}$ is significantly different from that of E_A . The numerical comparison of mappings produced by minimizing $E_{\mathbb{A}}$ versus E_A is presented in Section 7.1.

In practice, the spherical simplicial mapping f is represented as a matrix

$$\mathbf{f} \equiv \begin{bmatrix} f_1^1 & f_1^2 & f_1^3 \\ \vdots & \vdots & \vdots \\ f_n^1 & f_n^2 & f_n^3 \end{bmatrix} \equiv [\mathbf{f}^1, \mathbf{f}^2, \mathbf{f}^3] \equiv \begin{bmatrix} \mathbf{f}_1^\top \\ \vdots \\ \mathbf{f}_n^\top \end{bmatrix},$$

where $\mathbf{f}_i \in \mathbb{S}^2$ for $i = 1, \dots, n$. From [35, Lemma 3.1], the stretch energy E_S can be expressed as

$$E_S(\mathbf{f}) = \sum_{s=1,2,3} \frac{1}{2} \mathbf{f}^s \top L_S(\mathbf{f}) \mathbf{f}^s$$

where $L_S(\mathbf{f})$ is the weighted Laplacian matrix,

$$[L_S(\mathbf{f})]_{i,j} \begin{cases} -\frac{1}{2} \left(\frac{\cot(\theta_{i,j}^k(\mathbf{f}))}{\sigma_{\mathbf{f}}([v_i, v_j, v_k])} + \frac{\cot(\theta_{j,i}^\ell(\mathbf{f}))}{\sigma_{\mathbf{f}}([v_j, v_i, v_\ell])} \right) & \text{if } [v_i, v_j] \in \mathcal{E}(\mathcal{M}) \\ -\sum_{\ell \neq i} [L_S(\mathbf{f})]_{i,\ell} & \text{if } j = i \\ 0 & \text{otherwise} \end{cases} \quad (4.9)$$

in which $\theta_{i,j}^k(\mathbf{f})$ is the angle opposite to the edge $[f_i, f_j]$ at the point f_k , as illustrated in Figure 3, and $\sigma_{\mathbf{f}}([v_i, v_j, v_k])$ is the stretch factor of f on the triangular face $[v_i, v_j, v_k]$ by

$$\sigma_{\mathbf{f}}([v_i, v_j, v_k]) = \frac{|[v_i, v_j, v_k]|}{|[f_i, f_j, f_k]|}.$$

As a result, the minimization of spherical authalic energy (4.1) is formulated as

$$\operatorname{argmin}_{\mathbf{f}_\ell \in \mathbb{S}^2} E_{\mathbb{A}}(\mathbf{f}) \equiv \frac{|\mathcal{M}|}{6 \mathcal{V}(\mathbf{f})} \sum_{s=1,2,3} \mathbf{f}^s \top L_S(\mathbf{f}) \mathbf{f}^s - 3 \mathcal{V}(\mathbf{f}). \quad (4.10)$$

In order to minimize $E_{\mathbb{A}}$, it is essential to derive the gradient formula, which will be introduced in the following section.

4.2 Reformulation with spherical coordinate

To remain vertices of simplicial mapping \mathbf{f} on the sphere during optimization, i.e. $\mathbf{f}_i \in \mathbb{S}^2$ for $i = 1, \dots, n$, we can represent \mathbf{f} by the spherical coordinate. In this section, we would derive the gradient of $E_{\mathbb{A}}$ for spherical coordinates to minimize the energy.

Specifically, \mathbf{f} can be represented as

$$\mathbf{f}^1 = \sin \boldsymbol{\theta} \odot \cos \boldsymbol{\phi}, \quad \mathbf{f}^2 = \sin \boldsymbol{\theta} \odot \sin \boldsymbol{\phi}, \quad \text{and} \quad \mathbf{f}^3 = \cos \boldsymbol{\theta}, \quad (4.11)$$

where \odot denotes the Hadamard product of vectors, $\boldsymbol{\theta} = (\theta_1, \dots, \theta_n)^\top$, and $\boldsymbol{\phi} = (\phi_1, \dots, \phi_n)^\top$. The inverse relation is

$$\boldsymbol{\theta} = \arccos(\mathbf{f}^3), \quad \boldsymbol{\phi} = \operatorname{atan2}(\mathbf{f}^2, \mathbf{f}^1), \quad (4.12)$$

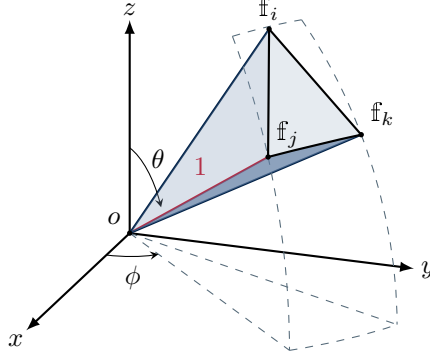


Fig. 4. An illustration for the tetrahedron $[o, \mathbb{f}_i, \mathbb{f}_j, \mathbb{f}_k]$ formed by the face $[\mathbb{f}_i, \mathbb{f}_j, \mathbb{f}_k]$ and the origin o of \mathbb{R}^3 .

where atan2 denotes the four-quadrant inverse tangent, $\theta_i \in [0, \pi]$, and $\phi \in (-\pi, \pi]$ for $i = 1, \dots, n$. Therefore, \mathbf{f} can be represented as

$$\mathbf{f} = \begin{bmatrix} \boldsymbol{\theta} \\ \boldsymbol{\phi} \end{bmatrix} \in \mathbb{R}^{2n} \quad (4.13)$$

The volume measurement $\mathcal{V}(\mathbf{f})$, as defined in (4.2), can be formulated by

$$\mathcal{V}(\mathbf{f}) = \sum_{[v_i, v_j, v_k] \in \mathcal{F}(\mathcal{M})} \frac{\mathbb{f}_i^\top (\mathbb{f}_j \times \mathbb{f}_k)}{6},$$

as illustrated in Figure 4. To compute the gradient of $|[o, \mathbb{f}_i, \mathbb{f}_j, \mathbb{f}_k]|$, we let $\tau = \{i, j, k\}$ and denote the x, y, and z-coordinate of \mathbb{f}_i , \mathbb{f}_j , and \mathbb{f}_k by

$$\begin{aligned} \mathbb{f}_\tau^1 &= \begin{bmatrix} \sin \theta_i \cos \phi_i \\ \sin \theta_j \cos \phi_j \\ \sin \theta_k \cos \phi_k \end{bmatrix} = \begin{bmatrix} \sin \theta_i \\ \sin \theta_j \\ \sin \theta_k \end{bmatrix} \odot \begin{bmatrix} \cos \phi_i \\ \cos \phi_j \\ \cos \phi_k \end{bmatrix} = \sin \boldsymbol{\theta}_\tau \odot \cos \boldsymbol{\phi}_\tau, \\ \mathbb{f}_\tau^2 &= \begin{bmatrix} \sin \theta_i \sin \phi_i \\ \sin \theta_j \sin \phi_j \\ \sin \theta_k \sin \phi_k \end{bmatrix} = \begin{bmatrix} \sin \theta_i \\ \sin \theta_j \\ \sin \theta_k \end{bmatrix} \odot \begin{bmatrix} \sin \phi_i \\ \sin \phi_j \\ \sin \phi_k \end{bmatrix} = \sin \boldsymbol{\theta}_\tau \odot \sin \boldsymbol{\phi}_\tau, \\ \mathbb{f}_\tau^3 &= \begin{bmatrix} \cos \theta_i \\ \cos \theta_j \\ \cos \theta_k \end{bmatrix} = \cos \boldsymbol{\theta}_\tau. \end{aligned}$$

Next, the gradient of $|[o, \mathbb{f}_i, \mathbb{f}_j, \mathbb{f}_k]|$ with respect to $\mathbb{f}_\tau^1, \mathbb{f}_\tau^2, \mathbb{f}_\tau^3$ is

$$\nabla_{\mathbb{f}_\tau^1} |[o, \mathbb{f}_i, \mathbb{f}_j, \mathbb{f}_k]| = \frac{1}{6} (\mathbb{f}_\tau^2 \times \mathbb{f}_\tau^3),$$

$$\nabla_{\mathbb{f}_\tau^2} |[o, \mathbb{f}_i, \mathbb{f}_j, \mathbb{f}_k]| = \frac{1}{6} (\mathbb{f}_\tau^3 \times \mathbb{f}_\tau^1),$$

$$\nabla_{\mathbb{f}_\tau^3} |[o, \mathbb{f}_i, \mathbb{f}_j, \mathbb{f}_k]| = \frac{1}{6} (\mathbb{f}_\tau^1 \times \mathbb{f}_\tau^2).$$

Then, by applying the chain rule, the gradient of $|[o, \mathbb{f}_i, \mathbb{f}_j, \mathbb{f}_k]|$ with respect to $\boldsymbol{\theta}_\tau$ and $\boldsymbol{\phi}_\tau$ is formulated as

$$\nabla_{\boldsymbol{\theta}_\tau} |[o, \mathbb{f}_i, \mathbb{f}_j, \mathbb{f}_k]| = \frac{1}{6} (\cos \boldsymbol{\theta}_\tau \odot \cos \boldsymbol{\phi}_\tau \odot (\mathbb{f}_\tau^2 \times \mathbb{f}_\tau^3) \quad (4.14a)$$

$$+ \cos \boldsymbol{\theta}_\tau \odot \sin \boldsymbol{\phi}_\tau \odot (\mathbb{f}_\tau^3 \times \mathbb{f}_\tau^1) \quad (4.14b)$$

$$- \sin \boldsymbol{\theta}_\tau \odot (\mathbb{f}_\tau^1 \times \mathbb{f}_\tau^2)), \quad (4.14c)$$

and

$$\nabla_{\boldsymbol{\phi}_\tau} |[o, \mathbb{f}_i, \mathbb{f}_j, \mathbb{f}_k]| = \frac{1}{6} (\sin \boldsymbol{\theta}_\tau \odot \cos \boldsymbol{\phi}_\tau \odot (\mathbb{f}_\tau^3 \times \mathbb{f}_\tau^1) \quad (4.14d)$$

$$- \sin \boldsymbol{\theta}_\tau \odot \sin \boldsymbol{\phi}_\tau \odot (\mathbb{f}_\tau^2 \times \mathbb{f}_\tau^3)). \quad (4.14e)$$

As a result, By assembling associated tetrahedra with the formulation in (4.14), the gradient of volume $\mathcal{V}(\mathbf{f})$ can be computed. We denote $\nabla_{\boldsymbol{\theta}}\mathcal{V}(\mathbf{f})$ and $\nabla_{\boldsymbol{\phi}}\mathcal{V}(\mathbf{f})$ as the gradient of $\mathcal{V}(\mathbf{f})$ with respect to $\boldsymbol{\theta}$ and $\boldsymbol{\phi}$.

From [35, Theorem 3.5], the gradient of $E_S(\mathbf{f})$ with respect to \mathbf{f} is

$$\nabla_{\mathbf{f}^s}E_S(\mathbf{f}) = 2L_S(\mathbf{f})\mathbf{f}^s, \quad \text{for } s = 1, 2, 3. \quad (4.15)$$

Therefore, regarding \mathbf{f} as $\mathbf{f}(\mathbf{f})$, by applying the chain rule again, the gradient of $E_{\mathbb{A}}$ with respect to \mathbf{f} is formulated as

$$\begin{aligned} \nabla_{\boldsymbol{\theta}}E_{\mathbb{A}}(\mathbf{f}) &= \left(\frac{|\mathcal{M}|}{\mathcal{V}(\mathbf{f})}\right)\nabla_{\boldsymbol{\theta}}E_S(\mathbf{f}) + \nabla_{\boldsymbol{\theta}}\left(\frac{|\mathcal{M}|}{\mathcal{V}(\mathbf{f})}\right)E_S(\mathbf{f}) - \nabla_{\boldsymbol{\theta}}(\mathcal{V}(\mathbf{f})) \\ &= \left(\frac{2|\mathcal{M}|}{\mathcal{V}(\mathbf{f})}\right)\left(\cos\boldsymbol{\theta} \odot \cos\boldsymbol{\phi} \odot L_S(\mathbf{f})\mathbf{f}^1 + \cos\boldsymbol{\theta} \odot \sin\boldsymbol{\phi} \odot L_S(\mathbf{f})\mathbf{f}^2\right. \\ &\quad \left. - \sin\boldsymbol{\theta} \odot L_S(\mathbf{f})\mathbf{f}^3\right) - \left(1 + \frac{|\mathcal{M}|E_S(\mathbf{f})}{\mathcal{V}(\mathbf{f})^2}\right)\nabla_{\boldsymbol{\theta}}\mathcal{V}(\mathbf{f}). \end{aligned} \quad (4.16a)$$

and

$$\begin{aligned} \nabla_{\boldsymbol{\phi}}E_{\mathbb{A}}(\mathbf{f}) &= \left(\frac{|\mathcal{M}|}{\mathcal{V}(\mathbf{f})}\right)\nabla_{\boldsymbol{\phi}}E_S(\mathbf{f}) + \nabla_{\boldsymbol{\phi}}\left(\frac{|\mathcal{M}|}{\mathcal{V}(\mathbf{f})}\right)E_S(\mathbf{f}) - \nabla_{\boldsymbol{\phi}}(\mathcal{V}(\mathbf{f})) \\ &= \left(\frac{2|\mathcal{M}|}{\mathcal{V}(\mathbf{f})}\right)\left(\sin\boldsymbol{\theta} \odot \cos\boldsymbol{\phi} \odot L_S(\mathbf{f})\mathbf{f}^2 - \sin\boldsymbol{\theta} \odot \sin\boldsymbol{\phi} \odot L_S(\mathbf{f})\mathbf{f}^1\right) \\ &\quad - \left(1 + \frac{|\mathcal{M}|E_S(\mathbf{f})}{\mathcal{V}(\mathbf{f})^2}\right)\nabla_{\boldsymbol{\phi}}\mathcal{V}(\mathbf{f}). \end{aligned} \quad (4.16b)$$

With this explicit gradient formula of $E_{\mathbb{A}}$ in (4.16), we develop a nonlinear CG method with appropriate preconditioning to solve (4.10), which will be thoroughly explained in the next section.

5 Preconditioned nonlinear CG method

The conjugate gradient (CG) method is an iterative method, proposed by Hestenes and Stiefel [17], to solve linear systems with a large positive definite coefficient matrix. It also can be adapted to solve nonlinear optimization problems, proposed by Fletcher and Reeves [12]. In this section, we introduce the algorithmic procedure of the nonlinear CG method to solve the objective problem (4.10) with suitable preconditioning and discuss its convergence.

5.1 Algorithmic procedure

Before applying our proposed method, we select the initial mapping by using the output of the fixed-point method [36, Algorithm 4.3] with several iterations. This method rapidly reduces energy in the initial stages but quickly attenuates and, in some cases, may even cause the energy to increase. Therefore, we limit this method to 15 iterations or stop as soon as the energy increases, followed by our proposed method.

To eliminate rotational freedom, we fix two points during optimization. Specifically, we compute the area ratio, $|f(\tau)|/|\tau|$, for the 1-ring of each vertex and select the two vertices closest to the mean of the 1-ring area ratio. For simplicity, the remaining points with spherical coordinates are still denoted as \mathbf{f} as in (4.13).

The CG method is a line search method, that means throughout the whole iterative procedure, $\mathbf{f}^{(k)}$ for $k \geq 0$, is updated with the step length $\alpha_k \in \mathbb{R}$ and the direction $\mathbf{p}^{(k)} \in \mathbb{R}^{2(n-1)}$,

$$\mathbf{f}^{(k+1)} \leftarrow \mathbf{f}^{(k)} + \alpha_k \mathbf{p}^{(k)}. \quad (5.1)$$

The initial direction of our preconditioned nonlinear CG method is the descent gradient with the preconditioner M ,

$$\mathbf{p}^{(0)} = -M^{-1}\mathbf{g}^{(0)}, \quad M = I_2 \otimes [L_S(\mathbf{f})] \quad (5.2)$$

in which $\mathbf{g}^{(0)}$ denoted the gradient $\nabla_{\mathbf{f}}E_{\mathbb{A}}(\mathbf{f}^{(0)})$ as in (4.16). Notice that the preconditioner M is a symmetric positive definite matrix (constructed by the submatrix of the Laplacian matrix

$L_S(f)$ with two vertices fixed), which leads to $\mathbf{p}^{(0)}$ being a descent direction. In practice, we perform the reordered Cholesky decomposition for $L_S(\mathbf{f})$ to solve the linear system efficiently. For the k th iteration for $k \geq 1$, we have an additional correction term by the previous direction $\mathbf{p}^{(k-1)}$ and coefficient β_k as

$$\mathbf{p}^{(k)} = -M^{-1}\mathbf{g}^{(k)} + \beta_k\mathbf{p}^{(k-1)}, \quad \beta_k = \frac{\mathbf{g}^{(k)\top}M^{-1}\mathbf{g}^{(k)}}{\mathbf{g}^{(k-1)\top}M^{-1}\mathbf{g}^{(k-1)}}. \quad (5.3)$$

In terms of the step length α_k , we consider the 1-dimensional function

$$\varphi(\alpha) = E_{\mathbb{A}}(\mathbf{f}^{(k)} + \alpha\mathbf{p}^{(k)}).$$

The ideal step length satisfies $\alpha = \operatorname{argmin} \varphi(\alpha)$, which cannot be explicitly formulated due to the complexity of E_S . Thus, we interpolate with a quadratic polynomial and approximate the ideal step length with the polynomial's minimizer [31, Section 3.5]. In particular, with initial guess α_{k-1} , the quadratic function $\zeta(\alpha)$ is formed by interpolating the three pieces of information

$$\begin{cases} \varphi(0) = E_{\mathbb{A}}(\mathbf{f}^{(k)}), \\ \varphi'(0) = \left. \frac{d}{d\alpha} E_{\mathbb{A}}(\mathbf{f}^{(k)} + \alpha\mathbf{p}^{(k)}) \right|_{\alpha=0} = \mathbf{p}^{(k)\top}\mathbf{g}^{(k)}, \\ \varphi(\alpha_{k-1}) = E_{\mathbb{A}}(\mathbf{f}^{(k)} + \alpha_{k-1}\mathbf{p}^{(k)}). \end{cases} \quad (5.4a)$$

Then, we obtain

$$\zeta(\alpha) = a\alpha^2 + b\alpha + c \equiv \left(\frac{\varphi(\alpha_{k-1}) - \varphi(0) - \alpha_{k-1}\varphi'(0)}{\alpha_{k-1}^2} \right) \alpha^2 + \varphi'(0)\alpha + \varphi(0). \quad (5.4b)$$

Therefore, α_k is selected by the minimizer of $\zeta(\alpha)$, which satisfies $\zeta'(\alpha) = 0$, given by

$$\alpha_k = -\frac{b}{2a}. \quad (5.4c)$$

It is noteworthy that if the α_k doesn't make energy sufficiently decrease, we may use the minimizer of $\zeta(\alpha)$ to be the initial guess and interpolate again. The pseudo-code of the proposed method can be summarized by the Algorithm 1.

Algorithm 1 Preconditioned nonlinear CG method for spherical authalic mapping

Require: A simplicial surface \mathcal{M} .

Ensure: A spherical authalic mapping \mathbb{f}^* .

- 1: Perform [36, Alg. 4.3] to 15 iterations
 - 2: Compute spherical coordinates $[\boldsymbol{\theta}, \boldsymbol{\phi}]$ by (4.12).
 - 3: Compute gradient \mathbf{g} by (4.16) with respect to \mathbf{f} .
 - 4: Compute the preconditioner M by (5.2).
 - 5: Perform Cholesky decompositions of M .
 - 6: Solve $M\mathbf{h} = \mathbf{g}$.
 - 7: Let $\mathbf{p} = -\mathbf{h}$.
 - 8: Let $\alpha = 0.01$.
 - 9: **while** not converge **do**
 - 10: Update α as (5.4).
 - 11: Update $\mathbf{f} \leftarrow \mathbf{f} + \alpha\mathbf{p}$.
 - 12: Let $\gamma = \mathbf{h}^\top\mathbf{g}$.
 - 13: Update the gradient \mathbf{g} (4.16).
 - 14: Solve $M\mathbf{h} = \mathbf{g}$.
 - 15: Update $\beta = (\mathbf{h}^\top\mathbf{g})/\gamma$.
 - 16: Update $\mathbf{p} \leftarrow -\mathbf{h} + \beta\mathbf{p}$.
 - 17: **end while**
 - 18: Obtain \mathbb{f}^* from \mathbf{f} by (4.11).
-

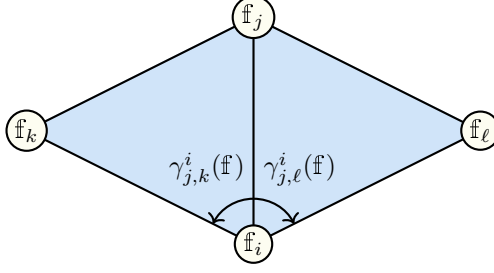


Fig. 5. An illustration of the mean value weight [13] defined on the surface $f(\mathcal{M})$.

5.2 Global convergence

The global convergence of the proposed method, Algorithm 1, is theoretically guaranteed under the assumption that each step length α_k in the algorithm is appropriately chosen to satisfy the strong Wolfe conditions,

$$E_I(\mathbf{f}^{(k+1)}) - E_I(\mathbf{f}^{(k)}) \leq c_1 \alpha_k \mathbf{g}^{(k)\top} \mathbf{p}^{(k)}, \quad (5.5a)$$

$$|\mathbf{g}^{(k+1)\top} \mathbf{p}^{(k)}| \leq c_2 |\mathbf{g}^{(k)\top} \mathbf{p}^{(k)}|, \quad (5.5b)$$

with $0 < c_1 < c_2 < \frac{1}{2}$, provided that $\mathbf{f}^{(k+1)} = \mathbf{f}^{(k)} + \alpha_k \mathbf{p}^{(k)}$ and $\mathbf{g}^{(k+1)}$ are the gradient of $\mathbf{f}^{(k+1)}$. Under this assumption, the following result holds:

Theorem 2. *The preconditioned nonlinear CG method, Algorithm 1, converges globally under the assumption of step lengths satisfying the strong Wolfe conditions (5.5) with $0 < c_1 < c_2 < \frac{1}{2}$.*

Proof. Since the objective functional $E_{\mathbb{A}}(\mathbf{f})$ is smooth, bounded below by 0, and the preconditioner M is a symmetric positive definite matrix (constructed from a submatrix of the Laplacian matrix), the proof follows directly from [25, Appendix A]. \square

6 Riemannian bijective correction

In Section 4.1, we modify the authalic energy E_A in (3.4) to the spherical authalic energy $E_{\mathbb{A}}$ in (4.1). This crucial modification significantly improves bijectivity, as confirmed by numerical comparisons in Section 7.1. To ensure bijectivity, we also proposed the Riemannian bijective correction as a post-processing step.

Specifically, we first construct the Laplacian matrix with mean value weight [13].

$$[L_M(\mathbb{f})]_{i,j} = \begin{cases} -\sum_{[v_i, v_j, v_k] \in \mathcal{F}(\mathcal{M})} \frac{\tan(\gamma_{j,k}^i(\mathbb{f})/2)}{\|\mathbb{f}_i - \mathbb{f}_j\|_2} & \text{if } [v_i, v_j] \in \mathcal{E}(\mathcal{M}), \\ -\sum_{\ell \neq i} [L_M(\mathbb{f})]_{i,\ell} & \text{if } j = i, \\ 0 & \text{otherwise,} \end{cases} \quad (6.1)$$

in which $\gamma_{j,k}^i(\mathbb{f})$ is the angle opposite to the edge $[\mathbb{f}_j, \mathbb{f}_k]$ at the point \mathbb{f}_i on $f(\mathcal{M})$ (see Figure 5). Next, consider a single folding triangle $\mathbf{F} = \{i, j, k\}$ and $\mathbf{F}^c = \{1, \dots, n\} \setminus \mathbf{F}$. The spherical points are projected onto the tangent plane with the normal vector $\mathbf{n} = (\mathbb{f}_i + \mathbb{f}_j + \mathbb{f}_k)/3$ as follows,

$$\tilde{\mathbb{f}} = \mathbb{h} - (\mathbb{h} \mathbf{n}) \mathbf{n}^\top + \mathbf{1} \mathbf{n}^\top, \quad \mathbb{h} = \mathbb{f} - \mathbf{1} \mathbf{n}^\top,$$

where $\mathbf{1} = (1, \dots, 1)^\top \in \mathbb{R}^n$. The folding triangular faces are then unfolded by solving the 3-by-3 linear system

$$[L_M(\mathbb{f})]_{\mathbf{F}, \mathbf{F}} \tilde{\mathbb{f}}_{\mathbf{F}}^s = -[L_M(\mathbb{f})]_{\mathbf{F}, \mathbf{F}^c} \tilde{\mathbb{f}}_{\mathbf{F}^c}^s, \quad \text{for } s = 1, 2, 3, \quad (6.2)$$

and projecting the corrected points $\tilde{\mathbb{f}}_{\mathbf{F}}$ back onto the sphere by normalizing the 2-norm

$$\mathbb{f}_{\mathbf{F}} = \frac{\tilde{\mathbb{f}}_{\mathbf{F}}}{\|\tilde{\mathbb{f}}_{\mathbf{F}}\|_2}.$$

Algorithm 2 Riemannian bijective correction for spherical mapping

Require: A simplicial surface \mathcal{M} and the spherical map \mathbf{f} .

Ensure: A bijective spherical map \mathbf{f}^* .

- 1: Compute the folding triangle's indices.
- 2: **while** # Folding > 0 **do**
- 3: Construct the mean value Laplacian L_M by (6.1).
- 4: **for** $k = 1, 2, \dots, \# \text{ Foldings}$ **do**
- 5: Select one folding index \mathbf{F} .
- 6: Set $\mathbf{F}^c = \{1, \dots, n\} \setminus \mathbf{F}$.
- 7: Compute the folding face center \mathbf{n} .
- 8: $\mathbf{h} = \mathbf{f} - \mathbf{n}^\top$.
- 9: $\mathbf{h} = \mathbf{h} - (\mathbf{h} \mathbf{n}) \mathbf{n}^\top + \mathbf{n}^\top$.
- 10: Solving the linear system

$$[L_M]_{\mathbf{F}, \mathbf{F}} \mathbf{h}_{\mathbf{F}}^s = -[L_M]_{\mathbf{F}, \mathbf{F}^c} \mathbf{h}_{\mathbf{F}^c}^s, \quad \text{for } s = 1, 2, 3.$$

- 11: Update $\mathbb{f}_{\mathbf{F}} = \mathbf{h}_{\mathbf{F}} / \|\mathbf{h}_{\mathbf{F}}\|_2$.
 - 12: **end for**
 - 13: **end while**
 - 14: Obtain \mathbf{f}^* from \mathbf{f} .
-

Note that only the 1-ring of the folding face affects the process in (6.2). Since local corrections may introduce folding triangles elsewhere, this procedure is repeated iteratively for all folding triangles until none remain.

The technique guarantees the unfolding of local folding faces, as in the planar case for open surfaces discussed in [35]. This is formalized in the following theorem:

Theorem 3. *Suppose the projection of the 1-ring of every folding face on the tangent plane is convex. Then, the solution of the linear system (6.2) is bijective.*

Proof. Let \mathbf{F} be a folding face. It suffices to show that the 1-ring of $\mathbb{f}_{\mathbf{F}}$ is bijective. We denote $\mathbb{N}_i = \{j \mid [v_i, v_j] \in \mathcal{E}(\mathcal{M})\}$ as the vertex indices of the 1-ring neighborhood of the vertex $v_i \in \mathcal{V}(\mathcal{M})$. From (6.2), for $i \in \mathbf{F}$,

$$\mathbb{f}_i = \sum_{\ell \in \mathbb{N}_i} \frac{-[L_M(\mathbb{f})]_{i, \ell}}{[L_M(\mathbb{f})]_{i, i}} \mathbb{f}_\ell.$$

The inequality $0 < \gamma_{j, k}^i(\mathbb{f}) < \pi$ implies that $\tan(\gamma_{j, k}^i(\mathbb{f})/2) > 0$. Therefore, the mean value weight in (6.1) is always positive so that $-[L_M(\mathbb{f})]_{i, \ell} > 0$ for $\ell \neq i$. This implies that $\frac{-[L_M(\mathbb{f})]_{i, \ell}}{[L_M(\mathbb{f})]_{i, i}} > 0$ and $\sum_{\ell \in \mathbb{N}_i} \frac{-[L_M(\mathbb{f})]_{i, \ell}}{[L_M(\mathbb{f})]_{i, i}} = 1$. Given the assumption that the projection of the 1-ring on the folding face \mathbf{F} is convex, it follows from [14, Theorem 4.1] that the 1-ring of $\mathbb{f}_{\mathbf{F}}$ is bijective. \square

The detailed procedure is summarized in Algorithm 2. It is worth noting that unfolding on the tangent plane ensures the local unfolding of the sphere. Notably, the normal vector of the tangent plane must correspond to the face center, rather than the folding triangle's normal vector, which may deviate significantly from the tangent plane of the sphere. Most importantly, this bijective correction numerically almost preserves bijective mappings and minimally affects area preservation in non-bijective cases.

7 Numerical experiments

This section presents the numerical results of the preconditioned nonlinear CG method (Algorithm 1) and the Riemannian bijective correction (Algorithm 2) for spherical authalic (area-preserving) parameterizations.

Figure 6 illustrates the benchmark triangular mesh models and their corresponding spherical authalic parameterizations. These benchmark models are sourced from established repositories, including the AIM@SHAPE shape repository [1], the Stanford 3D Scanning Repository [2], and

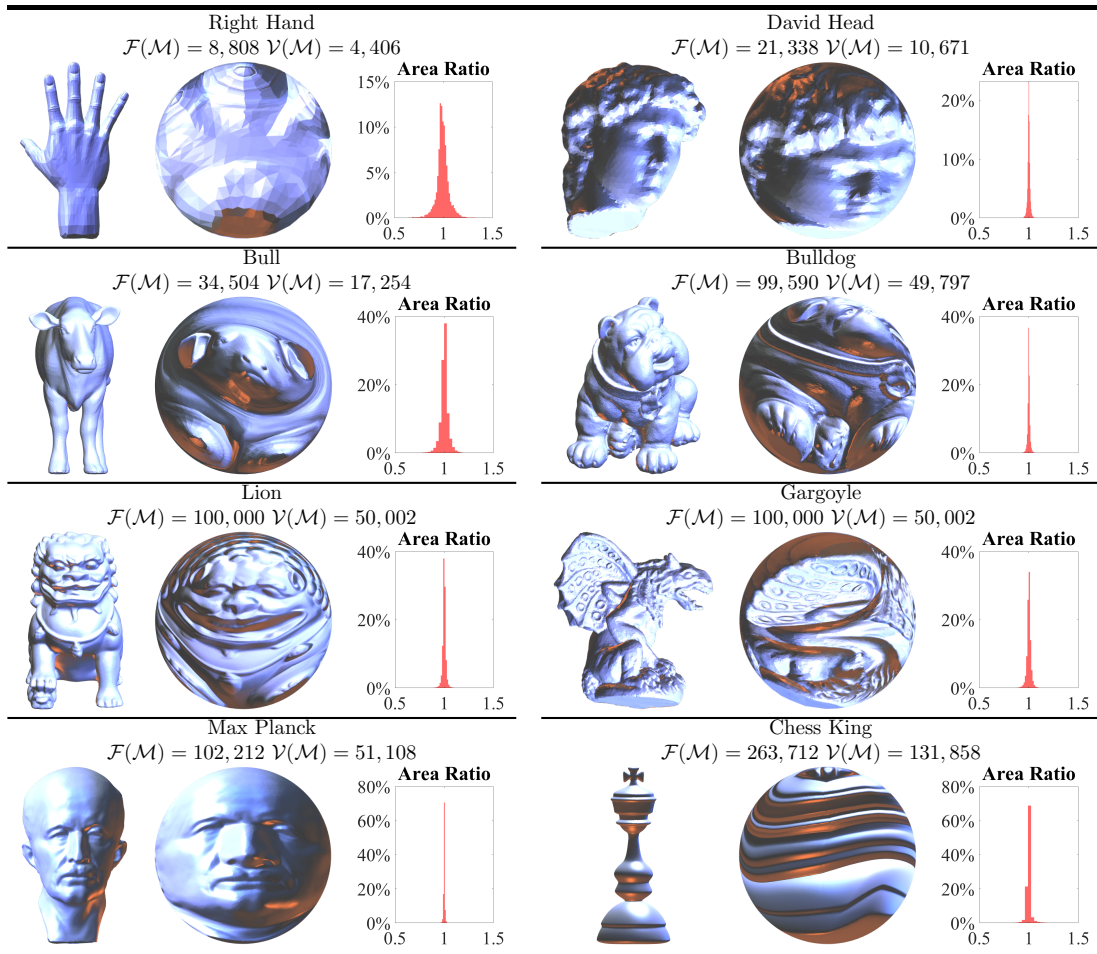


Fig. 6. The benchmark triangular mesh models, associated spherical area-preserving parameterization, and histogram of area ratio (7.1) produced by our proposed method.

Sketchfab [3]. Some models were modified to ensure that each triangular face contains at least one interior vertex. All experiments were conducted in MATLAB on a laptop with an AMD Ryzen 9 5900HS processor and 32 GB of RAM.

In the following subsections, we quantify the local area distortion with the area ratio:

$$\mathcal{R}_{\text{area}}(\tau) = \left| \frac{|f(\tau)|/|f(\mathcal{M})|}{|\tau|/|\mathcal{M}|} \right|. \quad (7.1)$$

The $\mathcal{R}_{\text{area}}$ of the spherical area-preserving parametrization by our proposed method is presented in Figure 6. The standard deviation of $\mathcal{R}_{\text{area}}$ is used to assess the area-preserving property because an ideal area-preserving mapping satisfies

$$\text{SD}_{\tau \in \mathcal{F}(\mathcal{M})} \mathcal{R}_{\text{area}}(\tau) = 0.$$

For consistency, we normalize the area of the surface \mathcal{M} to 4π ensuring the mean of $\mathcal{R}_{\text{area}}$ close to 1 in all cases. The global area distortion is quantified with the authalic energy E_A , defined by (3.4). As discussed in Section 3.2, the $E_A(f) = 0$ if f is perfectly area-preserving.

7.1 Spherical authalic energy and bijective correction

As discussed in Section 4.1, the modification from E_A to $E_{\mathbb{A}}$ is crucial for ensuring the bijectivity of the resulting mappings. To evaluate its efficacy, we conduct numerical experiments comparing the minimization of $E_{\mathbb{A}}$ versus E_A . However, as mentioned in Section 6, this modification alone may not completely eliminate folding triangles in challenging cases. Thus, the Riemannian bijective correction is applied as a post-processing step to achieve bijective mappings.

The results are summarized in Table 1. As expected, minimizing $E_{\mathbb{A}}$ significantly reduces the number of folding triangles compared to minimizing E_A . Remarkably, in the case of E_A , the Riemannian bijective correction successfully eliminates all folding triangles, even for as many as 381 folding triangles in the Chess King mesh. Furthermore, minimizing $E_{\mathbb{A}}$ shows slightly better area-preserving properties in terms of E_A and standard deviation of $\mathcal{R}_{\text{area}}$ compared to minimizing E_A .

In conclusion, the results highlight the significance of minimizing $E_{\mathbb{A}}$ and the effectiveness of the Riemannian bijective correction.

Table 1. Numerical results comparing the minimization of $E_{\mathbb{A}}$ (4.1) and E_A (3.4) across benchmark triangular meshes. $\mathcal{R}_{\text{area}}$: area ratio (7.1); #Foldings: number of folding triangles.

Model name	minimize $E_{\mathbb{A}}^{\dagger}$				minimize E_A^{\dagger}			
	Time (secs.)	E_A	$\mathcal{R}_{\text{area}}$ SD	#Foldings	Time (secs.)	E_A	$\mathcal{R}_{\text{area}}$ SD	#Foldings*
Right Hand	0.75	2.44×10^{-2}	6.77×10^{-2}	0	0.91	2.67×10^{-1}	2.06×10^{-1}	165 \rightarrow 0
David Head	0.72	2.12×10^{-3}	1.28×10^{-2}	0	0.93	3.65×10^{-3}	1.70×10^{-2}	0
Bull	3.57	2.28×10^{-2}	5.24×10^{-2}	0	3.87	2.21×10^{-1}	1.38×10^{-1}	18 \rightarrow 0
Bulldog	9.93	1.90×10^{-3}	1.57×10^{-2}	0	4.59	3.01×10^{-2}	4.98×10^{-2}	0
Lion Statue	15.73	5.81×10^{-3}	2.14×10^{-2}	0	14.82	9.57×10^{-2}	8.48×10^{-2}	11 \rightarrow 0
Gargoyle	15.97	3.83×10^{-3}	2.12×10^{-2}	0	7.23	1.66×10^{-2}	3.89×10^{-2}	0
Max Planck	4.73	9.51×10^{-4}	9.35×10^{-3}	0	2.58	2.49×10^{-2}	4.48×10^{-2}	0
Chess King	46.61	1.98×10^{-2}	3.90×10^{-2}	0	64.68	6.89×10^{-2}	7.27×10^{-2}	381 \rightarrow 0

* left: before bijective correction; right: after bijective correction (Alg. 2)

† stopping criteria: energy deficit $< 10^{-5}$ or reach 100 iterations (Alg. 1)

7.2 Comparison to state-of-the-art methods

We next compare our proposed method (SAEM) with the spherical density-equalizing mapping (SDEM) [28] and the Riemannian gradient descent [33]. RGD has demonstrated superior area preservation compared to the fixed-point method [36], adaptive area-preserving mapping [6], and optimal transportation mapping [10], as reported in [33].

The numerical results are summarized in Table 2. In terms of computational efficiency, our proposed method outperforms the tested methods in most cases (see Figure 7 left). The inefficiency of SDEM likely stems from solving a large-scale linear system for the PDE and

bijjective correction in each iteration. Both our method and the RGD method are line search methods, resulting in comparable efficiency.

In terms of accuracy, both E_A and the standard deviation of $\mathcal{R}_{\text{area}}$ indicate that our proposed method achieves superior area-preserving performance (see Figure 7 right). The poor accuracy of the RGD method may be due to the intrinsic limitations of gradient descent. Additionally, the bijjective correction in SDEM likely enhances angle preservation, which can interfere with area preservation.

Furthermore, both our Riemannian bijjective correction method and the manipulation of the Beltrami coefficient in SDEM demonstrate robust bijjectivity. In contrast, the stereographic projection-based bijjective correction in the RGD method fails to resolve folding triangles in certain challenging cases.

To clearly demonstrate the improvements of our proposed method, Figure 8 presents the ratios of the results from RGD and SDEM to those of our method across the metrics in Table 2, including computational time, authalic energy E_A , and the standard deviation of $\mathcal{R}_{\text{area}}$. A ratio of 1 indicates equivalent performance, while a ratio greater than 1 signifies the superiority of our algorithm. The results emphasize the outstanding performance of our method compared to state-of-the-art methods.

In summary, our proposed method outperforms the RGD method and SDEM in terms of efficiency, accuracy, and bijjectivity.

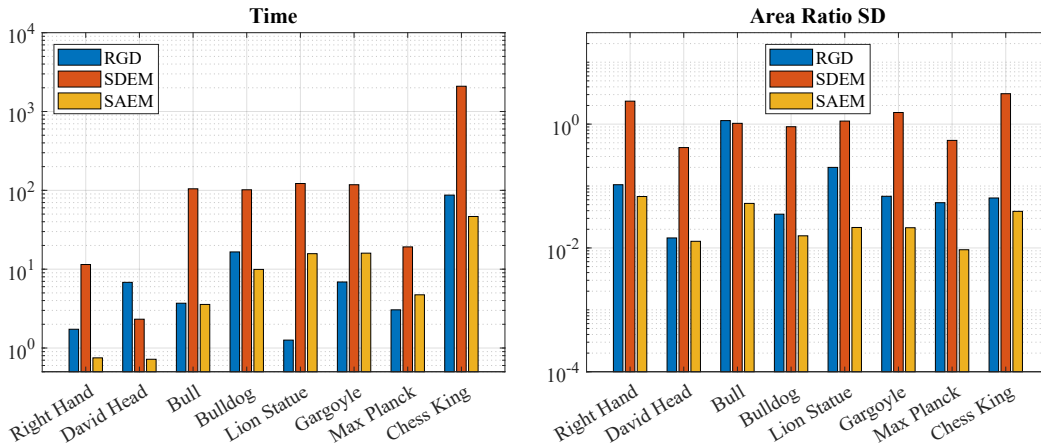


Fig. 7. The numerical results of our proposed method (SAEM), Riemannian gradient descent (RGD) [33], and spherical density-equalizing mapping (SDEM) [28]. Left: computational time cost; Right: standard deviation of area ratio (7.1).

8 Discussion

In this section, we discuss key differences in methods for mapping vertices onto a sphere, strategies for ensuring bijjectivity, and previous studies on SEM for area-preserving mappings on genus-zero surfaces.

8.1 Computational methods for spherical authalic mappings

There are several approaches for maintaining the vertices of an authalic map on a sphere. The first approach treats the sphere as a plane using stereographic projection. Nadeem et al. [30] and Choi et al. [6] address the area-preserving mapping problem through optimal mass transport. Starting with an initial spherical conformal mapping, they apply stereographic projection to the plane and solve the problem using the Newton method. Similarly, Yueh et al. [36] employ stereographic projection and the fixed-point method to update the unit disk for the southern hemisphere while handling the northern hemisphere through inversion to achieve spherical area-preserving mappings.

The second approach is Riemannian optimization, where points are projected onto the tangent plane and subsequently normalized onto the sphere using the 2-norm, adhering to the

Table 2. Numerical results of spherical authalic energy minimization (SAEM), Riemannian gradient descent (RGD) [33], and spherical density-equalizing mapping (SDEM) [28]. E_A : authalic energy (3.4); $\mathcal{R}_{\text{area}}$: area ratio (7.1); #Foldings: number of folding triangles; #Iterations: iteration count.

Metric	Model name	Spherical authalic energy minimization (SAEM) [†]	Riemannian gradient descent (RGD) [‡] [33]	Spherical density-equalizing mapping (SDEM) [§] [28]
Time	Right Hand	0.75	1.73	11.46
	David Head	0.72	6.81	2.32
	Bull	3.57	3.70	104.62
	Bulldog	9.93	16.55	101.65
	Lion	15.73	1.26	122.10
	Gargoyle	15.97	6.88	117.84
	Max Planck	4.73	3.05	19.17
	Chess King	46.61	87.03	2094.42
E_A	Right Hand	2.44×10^{-2}	8.12×10^{-2}	5.54×10^1
	David Head	2.12×10^{-3}	2.60×10^{-3}	2.22×10^0
	Bull	2.28×10^{-2}	2.40×10^{-1}	2.17×10^1
	Bulldog	1.90×10^{-3}	1.31×10^{-2}	1.04×10^1
	Lion	5.81×10^{-3}	4.79×10^{-1}	1.72×10^0
	Gargoyle	3.83×10^{-3}	5.14×10^{-2}	3.17×10^1
	Max Planck	9.51×10^{-4}	3.54×10^{-2}	3.61×10^0
	Chess King	1.98×10^{-2}	5.38×10^{-2}	1.22×10^2
$\mathcal{R}_{\text{area}}$ SD	Right Hand	6.77×10^{-2}	1.05×10^{-1}	2.35×10^0
	David Head	1.28×10^{-2}	1.45×10^{-2}	4.18×10^{-1}
	Bull	5.24×10^{-2}	1.14×10^0	1.03×10^0
	Bulldog	1.57×10^{-2}	3.51×10^{-2}	9.08×10^{-1}
	Lion	2.14×10^{-2}	2.00×10^{-1}	1.12×10^0
	Gargoyle	2.12×10^{-2}	6.88×10^{-2}	1.54×10^0
	Max Planck	9.53×10^{-3}	5.38×10^{-2}	5.46×10^{-1}
	Chess King	3.90×10^{-2}	6.41×10^{-2}	3.10×10^0
# Foldings	Right Hand	0	0	0
	David Head	0	0	0
	Bull	0	3	0
	Bulldog	0	0	0
	Lion	0	0	0
	Gargoyle	0	0	0
	Max Planck	0	0	0
	Chess King	0	17	0
# Iterations	Right Hand	100*	127	50*
	David Head	90	200*	26
	Bull	100*	50	50*
	Bulldog	56	60	50*
	Lion	100*	2	50*
	Gargoyle	100*	17	50*
	Max Planck	24	8	23
	Chess King	100*	107	50*

* indicates reaching the maximum iteration limit.

[†] stopping criteria: energy deficit $< 10^{-5}$ or reach 100 iterations

[‡] stopping criteria: energy deficit $< 5 \times 10^{-6}$ or reach 200 iterations

[§] stopping parameter = 10^{-3} , maximum iterations = 50.

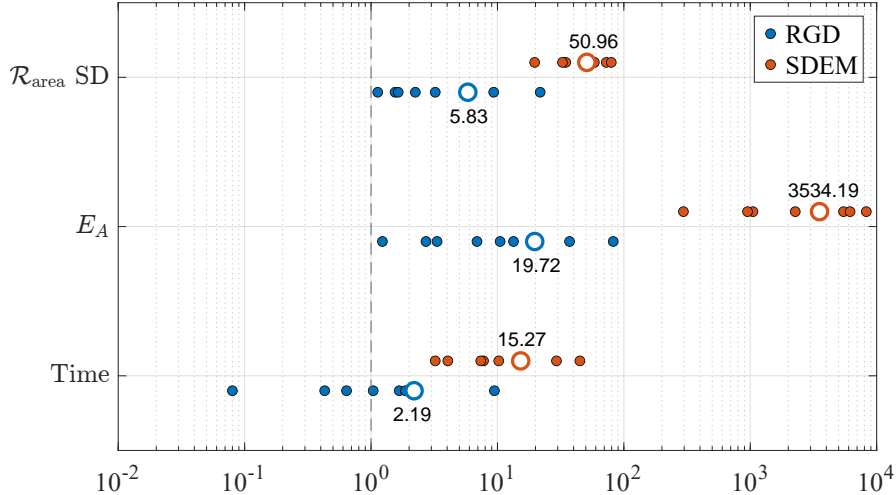


Fig. 8. The ratio of the results from Riemannian gradient descent (RGD) [33] and spherical density-equalizing mapping (SDEM) [28] to those of our method (SAEM). The big circle indicates the average of the ratios. E_A : authalic energy (3.4); $\mathcal{R}_{\text{area}}$: area ratio (7.1).

principles of Riemannian geometry as a generalization of Euclidean space. Lyu et al. [28] use the area ratio as a density function, achieving area preservation by solving the diffusion equation with an initial spherical conformal mapping, and incorporating Riemannian optimization into the diffusion process. Sutti and Yueh [33] apply the Riemannian gradient descent method for energy minimization, offering better theoretical convergence than projected gradient descent.

The final approach addresses the problem directly in the sphere. Instead of working in Euclidean space, Cui et al. [10] solve the optimal transportation map using Newton’s method on the sphere. In our work, we adopt spherical coordinates and implement the preconditioned nonlinear CG method.

8.2 Spherical bijective correction

In the work of Lyu et al. [28], they manipulate the Beltrami coefficients μ to unfold triangles, as $\|\mu\|_\infty < 1$ ensures bijectivity for continuously differentiable mappings. However, this approach can be inefficient since they adjust μ in each iteration. Furthermore, the mapping associated with $\|\mu\|_\infty < 1$ is quasi-conformal, whose angle preservation may interfere with area preservation, leading to greater area distortion.

In the planar region, due to the bijectivity of convex combination mappings, bijectivity is ensured by solving a linear system [35] with a mean value weight Laplacian matrix [14]. Numerically, it has negligible impact on bijective mappings and has minimal impact on area preservation in non-bijective cases.

To extend the unfolding method to the spherical mappings, Sutti and Yueh [33] combine the stereographic projection with the original algorithm [35]. While this approach successfully resolves the folding triangles in the plane, it often fails to unfold them on the sphere. In contrast, Yueh et al. [36] address this issue by locally resolving each folding triangle on the sphere. Due to the convex combination mappings being bijective in a planar region, in this work, we modify this method by resolving folding triangles on the tangent plane instead.

8.3 SEM-based methods

The minimization of stretch energy for disk-shaped area-preserving mappings was first introduced in [39] using the fixed-point method. This approach was later extended to spherical cases by applying stereographic projection and performing updates on the plane. Numerically, this method lacks theoretical convergence, occasionally even increasing energy in some challenging cases.

Inspired by this, Sutti and Yueh [33] used the output mapping as an initial solution and applied the Riemannian gradient descent method. Although this modification resolved convergence

issues, it still has limitations: gradient descent is intrinsically inefficient, the chosen objective functional may not ensure an area-preserving minimizer (it should follow (3.4), as shown in [25, Theorem 1]), and the inclusion of the image area term would cause folding triangles during optimization (see Section 4.1 in detail).

In this work, we approximate the signed image area term by a continuous formulation, which significantly improves the bijectivity of the produced mappings. To improve the efficiency, we develop the associated preconditioned nonlinear CG method to effectively compute a desired spherical area-preserving map.

9 Conclusion

In this paper, we have proposed a new objective functional modified from the original authalic energy. The new objective functional has the advantage that the bijectivity of the mapping is well preserved during the minimization process compared to the original authalic energy. To effectively achieve a minimizer, we developed the associated preconditioned nonlinear CG method with theoretically guaranteed convergence. Numerical experiments indicate that our new algorithm has significant improvement in both efficiency and accuracy compared to other state-of-the-art methods. To ensure the bijectivity of the produced mappings, we have proposed a Riemannian bijective correction as an optional postprocessing method, which has strong theoretical support under mild assumptions.

References

- [1] Digital Shape Workbench - Shape Repository. <http://visionair.ge.imati.cnr.it/ontologies/shapes/>, (2016).
- [2] The Stanford 3D Scanning Repository. <http://graphics.stanford.edu/data/3Dscanrep/>, (2016).
- [3] Sketchfab. <https://sketchfab.com/>, (2019).
- [4] S. Angenent, S. Haker, A. Tannenbaum, and R. Kikinis. Conformal geometry and brain flattening. In C. Taylor and A. Colchester, editors, *Medical Image Computing and Computer-Assisted Intervention – MICCAI’99*, pages 271–278, Berlin, Heidelberg, 1999. Springer Berlin Heidelberg.
- [5] S. Angenent, S. Haker, A. Tannenbaum, and R. Kikinis. On the Laplace-Beltrami operator and brain surface flattening. *IEEE Trans. Med. Imaging*, 18(8):700–711, 1999.
- [6] G. P. T. Choi, A. Giri, and L. Kumar. Adaptive area-preserving parameterization of open and closed anatomical surfaces. *Computers in Biology and Medicine*, 148:105715, 2022.
- [7] G. P.-T. Choi, K. T. Ho, and L. M. Lui. Spherical conformal parameterization of genus-0 point clouds for meshing. *SIAM Journal on Imaging Sciences*, 9(4):1582–1618, 2016.
- [8] G. P. T. Choi and C. H. Rycroft. Density-equalizing maps for simply connected open surfaces. *SIAM J. Imag. Sci.*, 11(2):1134–1178, 2018.
- [9] P. T. Choi, K. C. Lam, and L. M. Lui. FLASH: Fast landmark aligned spherical harmonic parameterization for genus-0 closed brain surfaces. *SIAM J. Imaging Sci.*, 8(1):67–94, 2015.
- [10] L. Cui, X. Qi, C. Wen, N. Lei, X. Li, M. Zhang, and X. Gu. Spherical optimal transportation. *Computer-Aided Design*, 115:181–193, 2019.
- [11] A. Dominitz and A. Tannenbaum. Texture mapping via optimal mass transport. *IEEE Trans. Vis. Comput. Graphics*, 16(3):419–433, 2010.
- [12] R. Fletcher and C. M. Reeves. Function minimization by conjugate gradients. *The Computer Journal*, 7(2):149–154, 1964.
- [13] M. S. Floater. Mean value coordinates. *Comput. Aided Geom. Des.*, 20(1):19–27, 2003.
- [14] M. S. Floater. One-to-one piecewise linear mappings over triangulations. *Math. Comput.*, 72(242):685–696, 2003.
- [15] M. S. Floater and K. Hormann. Surface parameterization: a tutorial and survey. In *Advances in Multiresolution for Geometric Modelling*, pages 157–186. Springer Berlin Heidelberg, 2005.
- [16] S. Haker, S. Angenent, A. Tannenbaum, R. Kikinis, G. Sapiro, and M. Halle. Conformal surface parameterization for texture mapping. *IEEE Trans. Vis. Comput. Graph.*, (2):181–189, 2000.
- [17] M. R. Hestenes, E. Stiefel, et al. *Methods of conjugate gradients for solving linear systems*, volume 49. NBS Washington, DC, 1952.
- [18] K. Hormann, B. Lévy, and A. Sheffer. Mesh parameterization: Theory and practice. In *ACM SIGGRAPH Course Notes*, 2007.
- [19] T.-M. Huang, W.-H. Liao, and W.-W. Lin. Fundamental theory and R-linear convergence of stretch energy minimization for spherical equiareal parameterization. *Journal of Numerical Mathematics*, 32(1):1–25, 2024.

- [20] K. C. Lam and L. M. Lui. Landmark-and intensity-based registration with large deformations via quasi-conformal maps. *SIAM J. Imag. Sci.*, 7(4):2364–2392, 2014.
- [21] W.-H. Liao, T.-M. Huang, W.-W. Lin, and M.-H. Yueh. Convergence of Dirichlet energy minimization for spherical conformal parameterizations. *Journal of Scientific Computing*, 98(1), 2023.
- [22] W.-W. Lin, C. Juang, M.-H. Yueh, T.-M. Huang, T. Li, S. Wang, and S.-T. Yau. 3D brain tumor segmentation using a two-stage optimal mass transport algorithm. *Sci. Rep.*, 11:14686, 2021.
- [23] W.-W. Lin, J.-W. Lin, T.-M. Huang, T. Li, M.-H. Yueh, and S.-T. Yau. A novel 2-phase residual U-net algorithm combined with optimal mass transportation for 3D brain tumor detection and segmentation. *Sci. Rep.*, 12:6452, 2022.
- [24] S.-Y. Liu, T.-M. Huang, W.-W. Lin, and M.-H. Yueh. Isovolumetric energy minimization for ball-shaped volume-preserving parameterizations of 3-manifolds, 2024. arXiv:2407.19272.
- [25] S.-Y. Liu and M.-H. Yueh. Convergent authalic energy minimization for disk area-preserving parameterizations. *J. Sci. Comput.*, 100(2):43, 2024.
- [26] L. M. Lui, K. C. Lam, S.-T. Yau, and X. Gu. Teichmüller mapping (t-map) and its applications to landmark matching registration. *SIAM J. Imag. Sci.*, 7(1):391–426, 2014.
- [27] Z. Lyu, G. P. T. Choi, and L. M. Lui. Bijective density-equalizing quasiconformal map for multiply connected open surfaces. *SIAM Journal on Imaging Sciences*, 17(1):706–755, 2024.
- [28] Z. Lyu, L. M. Lui, and G. P. T. Choi. Spherical density-equalizing map for genus-0 closed surfaces. *SIAM Journal on Imaging Sciences*, 17(4):2110–2141, 2024.
- [29] J. Moser. On the volume elements on a manifold. *Transactions of the American Mathematical Society*, 120(2):286–294, 1965.
- [30] S. Nadeem, Z. Su, W. Zeng, A. Kaufman, and X. Gu. Spherical parameterization balancing angle and area distortions. *IEEE Trans. Vis. Comput. Graphics*, 23(6):1663–1676, 2017.
- [31] J. Nocedal and S. J. Wright. *Numerical Optimization*. Springer, New York, NY, New York, NY, USA, 2e edition, 2006.
- [32] A. Sheffer, E. Praun, and K. Rose. Mesh parameterization methods and their applications. *Found. Trends. Comp. Graphics and Vision.*, 2(2):105–171, 2006.
- [33] M. Sutti and M.-H. Yueh. Riemannian gradient descent for spherical area-preserving mappings. *AIMS Math.*, 9(7):19414–19445, 2024.
- [34] Y. Yoshiyasu, W.-C. Ma, E. Yoshida, and F. Kanehiro. As-conformal-as-possible surface registration. In *Comput. Graph. Forum*, volume 33, pages 257–267. Wiley Online Library, 2014.
- [35] M.-H. Yueh. Theoretical foundation of the stretch energy minimization for area-preserving simplicial mappings. *SIAM J. Imaging Sci.*, 16(3):1142–1176, 2023.
- [36] M.-H. Yueh, T. Li, W.-W. Lin, and S.-T. Yau. A novel algorithm for volume-preserving parameterizations of 3-manifolds. *SIAM J. Imag. Sci.*, 12(2):1071–1098, 2019.
- [37] M.-H. Yueh, T. Li, W.-W. Lin, and S.-T. Yau. A new efficient algorithm for volume-preserving parameterizations of genus-one 3-manifolds. *SIAM J. Imag. Sci.*, 13(3):1536–1564, 2020.
- [38] M.-H. Yueh, W.-W. Lin, C.-T. Wu, and S.-T. Yau. An efficient energy minimization for conformal parameterizations. *J. Sci. Comput.*, 73(1):203–227, 2017.
- [39] M.-H. Yueh, W.-W. Lin, C.-T. Wu, and S.-T. Yau. A novel stretch energy minimization algorithm for equiareal parameterizations. *J. Sci. Comput.*, 78(3):1353–1386, 2019.
- [40] X. Zhao, Z. Su, X. D. Gu, A. Kaufman, J. Sun, J. Gao, and F. Luo. Area-preservation mapping using optimal mass transport. *IEEE Trans. Vis. Comput. Gr.*, 19(12):2838–2847, 2013.